Seasonal and Tidal Variations in Hydrologic Inputs Drive Salt Marsh Porewater Nitrate Dynamics

Emilio Grande[1,2], Erin C. Seybold[3], Corianne Tatariw[4], Ate Visser[5], Anna Braswell[6, 7], Bhavna Arora[8], François Birgand[9], John Haskins[10], Margaret Zimmer[1]

[1] University of California Santa Cruz, Department of Earth and Planetary Sciences
[2] California State University East Bay, Department of Earth and Environmental Sciences
[3] University of Kansas, Kansas Geological Survey
[4] University of Alabama, Department of Biological Sciences
[5] Lawrence Livermore National Laboratory, Nuclear and Chemical Sciences Division
[6] University of Florida, School of Forest Resources and Conservation, Fisheries and Aquatic Sciences Program
[7] Florida Sea Grant, Institute of Food and Agricultural Sciences
[8] Lawrence Berkeley National Laboratory, Energy Geosciences Division
[9] North Carolina State University, Department of Biological and Agricultural Engineering
[10] Elkhorn Slough National Estuarine Research Reserve

Corresponding author: Emilio Grande, California State University East Bay, 25800 Carlos Bee Blvd, Hayward, CA 94542, emilio.grande@csueastbay.edu

Abstract:

Salt marshes remove terrestrially derived nutrients en route to coasts. While these systems play a critical role in improving water quality, we still have a limited understanding of the spatiotemporal variability of biogeochemically reactive solutes and processes within salt marshes. We implemented a high-frequency sampling system to monitor sub-hourly nitrate (NO_3^-) concentrations in salt marsh porewater at Elkhorn Slough in central California, USA. We instrumented three marsh positions along an elevation gradient subjected to different amounts of tidal inundation, which we predicted would lead to varied biogeochemical characteristics and hydrological interactions. At each marsh position, we continuously monitored porewater NO_3^-

concentrations at depths of 10, 30, and 50 cm and porewater levels measured at 70 cm depth over seven deployments of ~10 days each that spanned seasonal wet/dry periods common to Mediterranean climates. We quantified tidal event hysteresis between NO_3^- and water level to understand how NO_3^- concentrations and sources fluctuate across tidal cycles. In dry periods, the NO_3^--porewater level relationship indicated that the NO_3^- source was likely estuarine surface water that flooded the transect during high tides and the salt marsh was a NO_3^- sink. In wet periods, the NO_3^--porewater level relationship suggested the salt marsh was a source of NO_3^-. These findings suggest that tidal and seasonal hydrologic fluxes together control NO_3^- porewater dynamics and export and influence ecological processes in coastal environments.

Keywords: Salt marsh hydrology, nitrate, hysteresis analysis, coastal hydrology, hydro-biogeochemistry, multi-scale nitrate dynamics, high frequency data

1. INTRODUCTION

Salt marsh systems act as buffers at the terrestrial-marine interface that retain or process terrestrially derived nutrients, potentially reducing the impacts of these pollutants on coastal environments (Reading *et al.*, 2017; Kumar *et al.*, 2019). However, in many salt marsh systems, elevated nutrient concentrations are exported to coastal areas following microbial processing, or in terrestrial fresh groundwater (Slomp and Van Cappellen, 2004; Gleeson *et al.*, 2013). These processes are critical to understand as excess nutrients, especially nitrate (NO_3^-), discharged to coastal estuaries can drive eutrophication and hypoxia (Peterson *et al.*, 2016), which may worsen with expected shifts in climatic patterns (Sinha *et al.*, 2017). Despite the importance of the biogeochemical reactivity of salt marshes, we do not have a complete understanding of the spatiotemporal variability of critical biogeochemically reactive solutes and processes. Specifically, there is a knowledge gap in the short-term dynamics of NO_3^- in porewater at timescales over which NO_3^- can be transported, retained, and removed.

Bidirectional water such as tidal water, shallow subsurface water (i.e., porewater), and terrestrial groundwater, are potential drivers of nutrient delivery and cycling in salt marsh porewater (Krause *et al.*, 2020). For example, water fluxes across the sediment-water interface control the exchange of nutrients, such as NO_3^-, from tidally-driven surface water into salt marsh porewater (Santos *et al.*, 2012; Wang *et al.*, 2022). However, the NO_3^- concentrations in salt marsh porewater at intra-tidal timescales and their relationship with porewater levels are not entirely understood (Caetano *et al.*, 2012). Available datasets of NO_3^- and other biogeochemical parameters in salt marshes are usually limited to short-term synoptic sampling campaigns or infrequent long-term sampling, often with limited spatial or temporal resolution. Therefore, we have historically understudied short-term and fine spatial scale porewater NO_3^- dynamics over more than a few tidal cycles in these ecosystems. For example, impacts of short-lived, episodic events such as storms and tidal inundation can drive biogeochemical parameters like redox potential (Grande *et al.*, 2022a), but may be missed by coarse resolution sampling.

Quantifying the dynamic relationship between tidal inundation and NO_3^- in salt marshes can improve our understanding of dominant NO_3^- transport pathways, as well as biogeochemical sources and retention processes. Previous work has found that the biogeochemical behavior of salt marshes can change as a function of tidal inundation, with shifts between retaining and producing NO_3^- during low neap and spring tides, respectively (Caetano *et al.*, 2012). However, these processes have not been quantified across multiple tidal cycles, seasons, or marsh types broadly. Thus, we lack an understanding how and when salt marshes transition from NO_3^- sources to sinks over tidal to seasonal time scales.

In riverine environments, solute concentration-discharge (i.e., c-Q) relationships have hysteretic behavior, which can be used to infer changing solute sources and transport processes (Chanat *et al.*, 2002; Arora *et al.*, 2020). Hysteresis occurs when the c-Q relationship is different on the rising limb of a storm hydrograph versus the falling limb (Chanat *et al.*, 2002; Aguilera and Melack, 2018). A clockwise relationship (NO_3^- concentrations are lower on the falling limb versus the rising limb) is thought to be the result of a limited NO_3^- supply close to the measurement location (Zuecco *et al.*, 2016). A counterclockwise hysteresis pattern occurs when the NO_3^- concentrations are higher on the falling limb versus the rising limb, and may be observed when the NO_3^- sources have a longer transport time (Bieroza and Heathwaite, 2015).

We propose to apply this analysis framework commonly used in riverine systems to better understand the general sources and sinks of NO_3^- during tidal events, for example, if NO_3^- is tidally sourced or if it is produced or consumed in the salt marsh. When applied to a salt marsh, hysteresis may occur when the NO_3^--porewater level relationship differs on the rising limb of the high tide versus the falling limb as the tide retreats. Several processes, including nitrification, denitrification, and dissimilatory nitrate reduction to ammonium, can increase or decrease NO_3^- concentrations in salt marshes over tidal cycles. We hypothesize that in salt marsh porewater, a clockwise loop indicates that the incoming tide is likely a source of NO_3^-, which is then consumed or diluted later in the tidal event. That is, as the tide floods the transect, infiltrating water into the marsh sediment, we would observe higher pore water NO_3^- concentrations in the rising versus the falling limb. Conversely, a counterclockwise loop with higher concentrations on the falling limb may indicate that the salt marsh could be a source of NO_3^- during ebbing tides or low tidal periods.

To advance our understanding of nutrient dynamics in salt marshes, we implemented a novel multiplexed pumping system coupled with a field-based spectrophotometer (spectro::lyser, S::CAN) to monitor sub-hourly porewater NO_3^- concentrations at multiple surface elevations and depths within a marsh (Birgand *et al.*, 2016). Specifically, we used the high spatiotemporal resolution NO_3^- data to study multi-scale hydrologic controls on marsh porewater NO_3^- concentration by investigating: (1) how tidal dynamics impact short-term (sub-hourly) variations in porewater NO_3^-; (2) how seasonality (i.e., wet versus dry seasons) modulates the impact of tidal cycles on NO_3^- dynamics; and (3) how potential NO_3^- sources and transport processes drive NO_3^- concentrations in salt marsh porewater.

2. STUDY AREA AND MEASUREMENTS

2.1- Study site description

This study was conducted at Elkhorn Slough in Monterey Bay, California (Figure 1A), which is part of the National Estuarine Research Reserve System (NERR). The principal sources of freshwater to Elkhorn Slough are the Old Salinas River, a perennial river that discharges at the mouth of the slough, and Carneros Creek, an intermittent stream that only flows during the wet winter months (Caffrey and Broenkow, 2002). Tides in the estuary are mixed semidiurnal with a mean range of 1.7 m, a spring tidal range of 2.5 m, and a neap tidal range of 0.9 m. The principal transport mechanism for surface water in Elkhorn Slough occurs via tidal exchange (Caffrey and Broenkow, 2002). Monterey Bay seawater reaches up to 10 km inland during high tides, and over 50% of the total water volume of the slough is flushed during each tidal cycle (Malzone, 1999).

Agricultural development in the watershed surrounding Elkhorn Slough increased in recent decades, leading to elevated nutrient concentrations, especially nitrogen species, in surface waters (Van Dop *et al.*, 2019). The Old Salinas River and Moro-Cojo Slough, a smaller estuary south of Elkhorn Slough (Figure 1A) drain intensely farmed areas and discharges at the southern end of Moss Landing Harbor (Caffrey *et al.*, 2002). These fertilizer-rich waters result in significant sources of NO_3^- at the mouth of Elkhorn Slough that are transported into the slough with the tides (Hicks *et al.*, 2019). The field site for the present study is located toward the upper section of the Slough (black star in Figure 1A). As surface water is transported from the mouth to these upper regions, we see elevated surface water NH_4^+ concentrations due to dissimilatory NO_3^- reduction to NH_4^+(DNRA), the anaerobic respiration by chemoorganoheterotroph microbes using NO_3^- as an electron acceptor for respiration and reducing NO_3^- to NH_4^+.(Caffrey *et al.*, 2002; Jeppesen *et al.*, 2018). Studies have also linked problematic surface water nutrient concentrations in Elkhorn Slough to climatic drivers, such as precipitation (Hicks *et al.*, 2019), with more significant NO_3^- and NH_4^+ concentration observed during rainy winter and spring months due to runoff from agricultural fields (Supporting information Figure S1). Finally, Elkhorn Slough has been designated as a moderately eutrophic estuary and high eutrophic expression close to the study site (Hughes *et al.*, 2011).

The average precipitation at Elkhorn Slough is 627 mm/year (based on 2001-2020 record collected by the NERR ~4.5 km from the study site), with ~ 90% of the precipitation falling between November and April as rain (Chapin *et al.*, 2004). Air temperature averages from 11.1 ^{o}C in the winter to 15.4 ^{o}C in the summer (Caffrey, 2002). The Mediterranean climate results in marked wet/dry seasonal dynamics (Figure 2), which provide the conditions to resolve seasonal variations in climatic forcing that impact subsurface saturation and biogeochemical conditions. In this area, the wet periods occur during the dormant winter season, while the dry periods occur during the summer growing season. Pickleweed, *Salicornia pacifica*, is the dominant marsh plant (Van Dyke and Wasson, 2005), and the dominant grazer and bioturbator is the lined shore crab, *Pachygrapsus crassipes* (Beheshti *et al.*, 2022).

To identify potential controls on the temporal variations in NO_3^- concentrations in subsurface marsh sediments, we used surface water pH, salinity, dissolved oxygen, temperature, and turbidity, available through the NERR. The NERR, in partnership with the National Oceanographic and Atmospheric Administration maintains a tidal gauge at the mouth of the slough (Figure 1A).

2.2- Experimental transect

For this study, we instrumented a 25 m experimental transect in an emergent tidal wetland with an elevation range of 0.24 m (Figure 1). We delineated the transect into upper, middle, and lower marsh positions through elevation surveys and inundation extents (supporting information Figure S2; Figure 1B). The elevations of the upper, middle, and lower marsh are 1.79 m, 1.65 m, and 1.55 m, respectively (all elevations are relative to NAVD88). These elevations are tidally inundated 6.7%, 8.9%, and 11.2% of the time, respectively, based on porewater level data collected at the site between February 2019 and November 2021. This wetland elevation categorization coincides with previous delineations of salt marsh zones across the Elkhorn Slough estuary based on vegetation coverage and elevation (Woolfolk and Labadie, 2012), and are thus broadly representative.

Sediment bulk density varied with elevation and depth at the site. Bulk density increased from the surface to 30 cm depth, then from 30 to 50 cm bulk density resembled that of the surface (Figure 1C). Sediment bulk density decreased from the upper marsh to the lower marsh positions, with mean values of 0.92 g/cm^3 and 0.22 g/cm^3, respectively.

We installed and maintained a network of observation wells at each marsh position to measure porewater level variations (Figure 1C). We installed the wells to a depth of 70 cm below the surface by pushing drive-point PVC pipes directly into the ground to minimize gaps around the pipe, which could cause water movement vertically along the well's annulus. We screened the wells from 5 cm below the ground surface to the total depth. We recorded water level and temperature in these wells with Solinst pressure transducer loggers (Grande *et al.*, 2022b; Ontario, Canada) at 5-minute intervals. We also measured air pressure at the transect at 5-minute intervals to barometrically correct the pressure transducer measurements to allow calculation of water level. We coupled these wells with high frequency measurements of porewater NO_3^- concentration using an *in-situ* sensor system described in the next section.

We installed a deep piezometer to 3.5 m below the ground surface, with 15-cm screen at the base, in an upland location ~5 m uphill from the upper marsh, which is not tidally inundated (Figure 2.1B). We used the same Solinst set up to measure groundwater levels at 5-minute intervals to quantify water level variations and evaluate the potential for fresh subsurface water to move laterally towards the salt marsh.

2.3- Water quality measurements

To measure high frequency variations in porewater NO_3^- concentration, we coupled a multisource pump system (MUX) with a field-based spectrophotometer (S::CAN Spectro::lyser™; (Birgand *et al.*, 2016; Liu *et al.*, 2020)). We connected the MUX to nine sampling cups installed to depths of 10, 30, and 50 cm at each marsh position (Figure 1C). We designed the sampling cups to be similar to those described in Liu *et al.*, (2021). The sampling cups are a “closed” chamber with an approximate volume of 150 mL (exact volume varied with the depth of the sampling cup), which held enough water to rinse the optical path and allow sufficient water for an accurate measurement (Birgand *et al.*, 2016). For each cup, we used a 6-8 cm length of 5 cm internal diameter (I.D.) screened PVC pipe capped at the bottom end with a PVC cap and an epoxy resin plug at its top end (supporting information Figure S3). We installed tubing (0.5 cm I.D.) from the bottom of the sampling cup through the sealed epoxy layer to connect the sampling cup to the MUX. We installed 51 micron in-line filters at the connection of the tubing with the MUX to reduce large particles from clogging the system, and minimize fouling potential in the MUX and the optical probe. For the sampling cups, we used an additional vent of equal internal diameter to prevent a vacuum forming during pumping, provide hydrostatic equilibrium with the surrounding water table in the cup, and provide an escape for air as water entered the cup (supporting information Figure S3). When installed, we placed washed sand around the sampling cups to avoid flow restriction towards the cups. Given the low permeability of the native sediment, we placed compacted native sediment above the sand layer to avoid sampling water from above the sampling cup depth.

The MUX pumped porewater from the sampling cups to a 4 mL quartz flow-through cuvette with a 10 mm pathlength (Starna-cell®, model 46-Q-10) attached to the optical probe (Figure 1C). We set the temporal resolution of NO_3^- concentration measurements to ~50 minutes for each measuring cycle. In each measuring cycle, we measured the empty cuvette (e.g., took an air absorbance measurement of the empty cuvette) to monitor any potential optic fouling of the cuvette over time (Etheridge *et al.*, 2014). We also flushed the cuvette with deionized water to remove chemical fouling once per measuring cycle. Lastly, we pumped and purged a cleaning solution (12 mg/L oxalic acid) to minimize the cuvette's chemical fouling during each sampling event. The MUX has logging capabilities and we stored the time stamp, the corresponding valve number, and absorbance measurement values from 200 nm to 737.5 nm (2.5 nm resolution) for each optical probe measurement. We deployed the optical sensor coupled with the MUX in seven deployment periods of ~ten days each, between January and October 2021 (Figure 2). Data gaps during deployments represent sampling cup or instrument malfunctions, resulting in different amounts of data for some marsh positions or depths (supporting information Table S1).

For this study, we also used available surface water quality data through the ESNERR. The closest sampling station to the research site is Kirby Park (2.1 km away; Figure 1A), where monthly surface water NO_3^- and NH_4^+ concentration data are available for the study period (January-October 2021).

3. METHODOLOGY

3.1- In situ nitrate measurements and data preparation

We developed a site-specific calibration model to estimate NO_3^- concentrations using the spectral data from the optical probe. Across all deployment periods, we collected a total of 91 grab samples as water flowed through the cuvette paired with the optical probe measurement. We analyzed these samples for NO_3^- concentration using a Lachat Quickchem 8500 auto-analyzer at the Marine Analytical Lab at the University of California, Santa Cruz, following the EPA 353.2 method (O'Dell, 1996). These samples comprised our calibration library, which we used in combination with the absorbance spectra from the optical probe to estimate NO_3^- using Partial Least Square Regression (PLSR; (Etheridge *et al.*, 2014) through the pls package in R (Liland *et al.*, 2021). This calibration model was then applied to the entire time series of absorbance spectra. A limitation of this work is the analytical uncertainty due to the low NO_3^- concentrations in the study area. However, the concentrations were above the NO_3^- detection limit (0.01 mg/L). Furthermore, more than 99% of the variance in laboratory measured NO_3^- concentration was explained by the sensor data. The Nash–Sutcliffe efficiency of the model was 0.88 and the root mean square error of the prediction was 0.09 mg/L (Supporting Information Figure S4). We generated NO_3^- concentration times series for each instrument deployment period using the calibration model. We filled short data gaps (<4 h) using cubic spline interpolation and produced a continuous time series to analyze tidal events.

To better capture the dimension and direction of NO_3^--porewater level relationship (i.e., get the water level and NO_3^- concentration datasets on the same time step), we used a locally estimated scatterplot smoothing (LOESS) with a minimal smoothing parameter (α) of 0.1 to smooth the NO_3^- concentration time series closely to the data (e.g., supporting information Figure S5).

3.2- Tidal events delineations

We delineated individual tidal events for each deployment, where tidal events were defined as the periods when the water level in the observation wells increased and then decreased as a function of individual tidal cycles (Figure 3). We considered tidal events only the tides that inundated the top of the salt marsh. Thus, we did not identify any tidal event during the May deployment because the site was never inundated (Supporting Information Table S1).

Differences in elevation across the salt marsh, where higher elevation sites were inundated less frequently, resulted in different numbers of tidal events at each marsh position. Furthermore, instrument failure during some deployments resulted in differences in the number of tidal events studied for individual depths and marsh positions. We delineated 158 tidal events, including 58 at the lower marsh, 43 at the middle marsh, and 57 at the upper marsh position.

Of the 158 tidal events, 65% occurred during the wet season (January to May 2021) and 35% occurred during the dry season (July to October 2021; Table S1).

3.3- Analyses of hysteresis indices

We used hysteresis indices to quantify temporal porewater NO_3^- concentration- porewater level relationships for each tidal event across marsh positions (Lloyd *et al.*, 2016). We used the porewater level measured in the observation wells at individual marsh positions (Figure 1C). The hysteresis index (*HI*) has been widely used, and there is a robust description of this analysis in the literature (Andrea *et al.*, 2006; Vaughan *et al.*, 2017; Liu *et al.*, 2021). In brief, the *HI* is based on normalized water level and NO_3^- concentration as:

$$h_{i-\,norm} = \frac{h_i - h_{min}}{h_{max} - h_{min}} \qquad (1)$$

$$C_{i-\,norm} = \frac{C_i - C_{min}}{C_{max} - Q_{min}} \qquad (2)$$

Where h_i and C_i are the water level and NO_3^- concentration values at time step *i*, h_{max} and h_{min} are the maximum and minimum water levels in the tidal event, and C_{max} and C_{min} are the maximum and minimum NO_3^- concentration in the tidal event. We normalized NO_3^- and water levels between 0 and 1 to facilitate the comparison of indices across tidal events because this ensures all events are evaluated on the same scale (Lloyd *et al.*, 2016).

Further, we calculated the *HI* for each water level interval (HI_j) as:

$$HI_j = C_{j-rising} - C_{j-falling} \qquad (3)$$

Where $C_{j-rising}$ and $C_{j-falling}$ are calculated by estimating C_{i-norm} at 1% intervals of h_{i-norm} on the rising and falling limbs through linear regression of two adjacent values C_{i-norm} (Vaughan *et al.*, 2017; Kincaid *et al.*, 2020). We calculated the mean HI_j value for each tidal event to determine an event-specific *HI* (Figure 4). The *HI* values ranged between −1 and 1. Negative values indicate counterclockwise hysteresis and positive values indicate clockwise hysteresis. The magnitude of *HI* is the normalized difference between the rising and falling limbs of a flooding high tide (Figure 4). *HI* close to zero represents less hysteresis (i.e., *HI'*s magnitude influences the size of the loop).

We also calculated Flushing Index values for each tidal event (*FI*, Figure 4C). The *FI* is computed as the slope of the line that intersects between the normalize NO_3^- concentrations at the peak tidal event (i.e., the maximum normalized porewater level value) and the normalized porewater level value at the beginning of the tidal event (Vaughan *et al.*, 2017). Values of this index range between −1 and 1 (Figure 4C). Negative values indicate a decrease in NO_3^- concentrations on the rising limb, whereas positive values indicate an increase in NO_3^- on the rising limb. The distance from zero indicates the magnitude of the difference in NO_3^- concentration at the start of the tidal event and the peak of the tidal event.

The FI is an indicator of the mechanism, in other words, the FI helps understanding if NO_3^- come into the marsh and sit there, or if it is drawn down by denitrification or dilution. A positive FI could suggest that the salt marsh is a source of NO_3^- or that tidal water "flushes" the salt marsh subsurface with high NO_3^-, and we observe it as an increase in NO_3^- on the rising limb of the event. A negative FI would imply that the tidal water is a source of NO_3^-, which is consumed in the salt marsh over the tidal event, resulting in a decrease in NO_3^- from the beginning of the high tide towards the maximum water level. A negative FI can also result from dilution processes if the incoming tidal water dilutes the salt marsh subsurface from the beginning to the peak of the tidal event.

3.4- Statistical tests

We analyzed the normality of all of the data distributions using histograms, Q-Q plots, and Shapiro-Wilk tests (Shapiro and Wilk, 1965) using the "shapiro.test" function in base R (R Core Team, 2021). We tested if the variations in porewater NO_3^- concentration differed significantly among marsh positions and depths using Levene's test (Schultz, 1985)"leveneTest" function from the "car" package in R (Fox and Weisberg, 2019). We used the Brown-Forsythe variant of the test, which uses deviations from the median because our data are non-parametric (Gastwirth *et al.*, 2009). We used the Kruskal-Wallis test (Breslow, 1970) to determine if hysteresis indices (*HI* and *FI*) differed between the wet and dry seasons and to evaluate differences in porewater NO_3^- concentration across depth and marsh positions. The Kruskal-Wallis test is a non-parametric method that tests the null hypothesis of identical populations. We used the "kruskal.test" function in base R (R Core Team, 2021) for this analysis. All significant results were further analyzed with pairwise Mann-Whitney U test (Rosner and Grove, 1999) to correct the significance level for multiple comparisons. For all analyses, P-values were used to determine significant differences between groups (α=0.05).

4. RESULTS

4.1- Precipitation, seasonal groundwater level and salt marsh porewater level fluctuations

Water year 2020 was extremely dry with 281 mm of total precipitation, which was 346 mm below the long-term annual average (627mm) for the area. Over the study period, we observed a difference of 1.34 m between the peak terrestrial groundwater level (2.75 m-amsl) in the wettest period (December 2020) and the lowest level (1.39 m-amsl) in the driest period (September 2021; Figure 2). The terrestrial water level responds to precipitation with relative increases during precipitation events (Figure 2).

Marsh porewater levels were subject to daily, biweekly, and seasonal tidal cycle inundation dynamics, resulting in multiple water level fluctuation frequencies (Grande *et al.*, 2022a). Porewater levels at the lower marsh position were consistently lower than at the upper and middle marsh positions during low tides, draining below the marsh surface elevation in each tidal cycle. However, the porewater level in the upper and middle marshes did not drop below the marsh elevation during the wet dormant season (e.g., January to March 2021; Figure 2). This indicates that this portion of the marsh does not drain substantially between daily tidal cycles during this period. As the system transitioned into the dry season, we observed that the terrestrial groundwater levels decreased, and the salt marsh porewater levels dropped below the salt marsh surface between tidal inundation periods (e.g., April to October 2021; Figure 2).

4.2- Effect of salt marsh position and depth on porewater nitrate concentrations

NO_3^- concentration in salt marsh porewater ranged between 0 and 0.99 mg/L over the study period, with a median of 0.16 mg/L (0.08 mg/L $\pm$ 0.24 mg/L 25 and 75 % quantiles, respectively). Overall, we found differences in NO_3^- concentrations across the marsh positions and depths, but these differences were complex and did not follow simple trends with marsh elevation. Temporal variations in NO_3^- concentration differed between marsh positions ($p < 0.0001$; Table 1; Figure 5A). The upper marsh position showed the most significant temporal variability (Interquartile range, IQR = 0.22 mg/L). However, the middle marsh had higher porewater NO_3^- concentrations (median = 0.19 mg/L) than the lower (0.14 mg/L) and upper marsh positions (0.14 mg/L; $p < 0.0001$; Table 1, Figure 5A).

Temporal variations in NO_3^- concentration also differed between depths ($p < 0.0001$; Figure 5B), with the 50 cm depth showing the greatest temporal variability across all marsh positions (IQR =

0.17 mg/L). The median NO_3^- concentration at 50 cm depth was significantly higher (0.19 mg/L) than the 10 cm (0.15 mg/L) and 30 cm depths (0.13 mg/L; $p < 0.0001$; Table 1, Figure 5B). The effect of depth on NO_3^- concentration varied between individual marsh positions, with the highest concentrations occurring at different depths in each position. At the lower marsh position, median NO_3^- concentration was highest at 30 cm depth (0.157 mg/L; $p < 0.0001$), and there was no difference between the 10 cm (0.134 mg/L) and 50 cm depths (0.133 mg/L; $p = 0.4$) (Table 2, Figure 5D). At the middle marsh, median NO_3^- concentration was lowest at the 50 cm depth (0.15 mg/L; $p < 0.0001$) and there was no difference between the 10 cm (0.21 mg/L) and 30 cm depths (0.23 mg/L; $p = 0.075$; Figure 5E). Finally, at the upper marsh, median NO_3^- concentrations varied between all depths, with the highest concentrations occurring at the 50 cm depth (0.27 mg/L) and the lowest at the 30 cm depth (0.06 mg/L; $p < 0.0001$; Figure 5F).

4.2.1 Seasonality of porewater nitrate concentration

Although the effect of marsh position and depth on NO_3^- concentrations was complex, we found clearer and more consistent differences between wet and dry periods. There were higher NO_3^- concentrations during wet periods (0.21 mg/L) than during dry periods (0.10 mg/L; $p < 0.0001$) across all marsh positions and depths (Figure 5G-H). However, the effect of wet/dry season on depth varied between individual marsh positions. At the lower and middle marsh positions, NO_3^- concentrations were higher at all depths during the wet season (Table 3). In contrast, at the upper marsh position, NO_3^- concentrations were lower at the 10 cm and 30 cm depths and higher at the 50 cm depth during the wet season (Table 3).

4.3- Estuarine surface water nitrate and ammonium concentrations

During the study period, monthly measurements of estuarine surface water NO_3^- concentration varied between 0.08 mg/L in summer (June 2021) and 2.9 mg/L in the winter (February 2021). Surface water NO_3^- had a mean, median, standard deviation, and interquartile range (IQR) of 0.46 mg/L, 0.13mg/L, 0.86mg/L, and 0.23 mg/L, respectively (Figure 5C).

Surface water NH_4^+ concentration varied between 0.06 mg/L in summer (June 2021) and 0.36 mg/L in the winter (February 2021). Surface water NH_4^+ had a mean, median, standard deviation, and IQR of 0.09 mg/L, 0.07 mg/L, 0.11 mg/L, and 0.07 mg/L, respectively (Figure 5C).

4.4 Hysteresis Index

Tidal event *HI* values were influenced by season (Figure 6C; $p < 0.0001$) rather than marsh position ($p = 0.3$) or depth ($p = 0.15$). Median *HI* was predominantly negative (counterclockwise) during the wet season (-0.13), contrasting with a predominantly positive (clockwise) *HI* during the dry season (0.15). However, this seasonal effect did not persist across all marsh positions and depths.

The effect of seasonality on hysteresis patterns was evident in the upper marsh position, with significant differences between wet and dry periods at all depths (Table 4). Predominantly positive *HI* in the dry season contrasted with predominantly negative *HI* in the wet season. There was no effect of season at any depth in the middle marsh position (Table 4). In the lower marsh, *HI* was negative during the wet season and positive during the dry season for the 10 cm and 50 cm depths, with significant differences among wet and dry periods (Table 4). Conversely, the *HI* in the 30 cm depth of the lower marsh was not significantly different among the dry and wet seasons (Table 4).

Variability in *HI* differed significantly between wet and dry periods for the middle marsh ($p = 0.015$) with the wet season displaying a larger distribution than the dry season (Figure 6). We did not find significant differences in the distribution between wet and dry seasons for the upper ($p = 0.7$) or lower ($p = 0.3$) marsh positions. Furthermore, we did not find any clear evidence that precipitation or tidal cycle influenced the distribution of the data (Figure S6). We also did not find any relationship between *HI* and estuarine water salinity, pH, dissolved oxygen, temperature, or turbidity (Figure S7).

4.5 Flushing Index

Similar to *HI*, *FI* was strongly affected by wet/dry seasonality. *FI* was predominantly positive during the wet season (median *FI* = 0.14) and predominantly negative during the dry season (median *FI*= -0.19; $p < 0.0001$; Figure 6A). The median *FI* was negative for the three marsh positions, with median *FI* values of -0.13, -0.15, and -0.14 for the lower, middle, and upper marsh positions, respectively, and there were no significant differences among the positions ($p = 1$). Similarly, we did not find significant differences between the 10, 30, and 50 cm depths, with median *FI* values of -0.13, -0.11, and -0.16, respectively ($p = 0.6$).

The effect of seasonality on *FI* was evident in individual salt marsh positions. In the lower marsh, predominantly negative *Fi*s during the dry season (-0.20) contrasted with positive *Fi*s during the wet season (0.11; $p = 0.001$). However, in the middle marsh, we did not find significant differences between the dry (median *FI* = -0.16) and wet seasons (median *FI* = 0.08; Kruskal-Wallis test: H= 0.27, df = 1, $p = 0.6$). In the upper marsh, we found significant differences in *FI* between dry (median *FI* = -0.19) and wet periods (median *FI* = 0.19; $p < 0.0001$).

The wet/dry seasonality effect on *FI* patterns was evident across depth for each individual marsh position (Table 4). In the upper marsh position, wet and dry season *Fi*s were significant at all depths (Table 4). In the middle marsh, the effect of seasonality was significant between wet and dry periods for the 10 cm, but not for the 30 or 50 cm depths (Table 4). The lower marsh position had significant differences between wet and dry periods for the 50 cm depth, but not for the 10 or 30 cm depths (Table 4).

Dispersion in *FI* differed significantly between wet and dry periods for the middle ($p < 0.001$) and upper ($p < 0.05$) marsh positions with the wet season displaying a larger distribution than the dry season (Figure 6). However, we did not find significant scattering for the lower marsh ($p = 0.4$). Moreover, we did not find any clear evidence that precipitation or tidal cycle influenced the distribution of the data (Figure S6). In addition, we did not find any relationship between *FI* and estuarine water salinity, pH, dissolved oxygen, temperature, or turbidity (Figure S8).

5. DISCUSSION

We combined high-frequency porewater NO_3^- concentration and porewater level time series data from a salt marsh to calculate NO_3^--porewater level hysteresis indices. We used these indices, which have been widely used in riverine systems (i.e., c-Q plots), to evaluate the effects of tidal forcings on marsh porewater biogeochemistry over short (tidal cycle) timescales to gain understanding of how seasonality in precipitation modulates this relationship. We explored how these hydrologic drivers (i.e., seasonal precipitation and tides) interact to produce seasonal patterns in subsurface chemistry that might influence nutrient export to coastal waters. We found strong evidence that wet/dry seasonal shifts in the salt marsh hydrology were associated with shifts in the NO_3^--porewater level hysteresis patterns. This analysis can help us understand the potential impacts of climate change, especially the predicted extreme changes in precipitation patterns in the western United States (Swain *et al.*, 2018), that might lead to significant shifts in the porewater NO_3^- concentration dynamics and marsh source/sink status.

5.1 Seasonal hydrologic drivers determine whether the marsh is a NO_3^- source or sink

Seasonal wet/dry regimes were the strongest driver of nitrate dynamics across the marsh platform, and set a baseline for functioning/behavior that was subsequently modified by tidal/intra-tidal cycles. The seasonal wet/dry regimes control shifts in the directionality of hysteresis between NO_3^- and porewater level, resulting in the marsh porewater being a net source for NO_3^- in the wet season and a net sink in the dry season (Figure 6).

While different marsh positions experience different inundation extents, the hysteresis index values indicate that all marsh positions display similar NO_3^--porewater level relationships (Figure 6). This finding is remarkable, considering that different marsh positions have distinct hydrologic pathways and differing degrees of terrestrial groundwater inputs (Robinson *et al.*, 2018). We had previously hypothesized that NO_3^- sources could range from mostly estuarine surface water in the lower marsh to a mix of tidally driven estuarine surface water, terrestrial groundwater, and surface runoff in the upper marsh. However, the hysteresis indices did not differ within the spatial extent of this work.

In the wet season, the hysteresis results generally imply NO_3^- enrichment occurred later in the tidal cycle, likely from distal, NO_3^--rich sources or *in situ* NO_3^- production (Figure 7). Specifically, we observed that the porewater NO_3^- concentration increased after the peak of a tidal event during the wet season. This could result from internal nitrogen cycling as tidal or porewater NH_4^+ is oxidized (i.e., nitrification). Additionally, terrestrial groundwater could be an external source of NO_3^- following a rise in the groundwater table (Figure 2), if the discharging groundwater is a NO_3^- source. In watershed hydrology, where these indices were developed, negative *HI*s and positive *FI*s have been described in golf courses and agricultural areas and were attributed to a rising water table during precipitation events, mobilizing NO_3^- from fertilizer applications stored in upper soil horizons (Oeurng *et al.*, 2010; Aguilera and Melack, 2018; Grande *et al.*, 2019). Our data suggest that similar 'transport' mechanisms may be mobilizing NO_3^- in coastal wetlands, although nitrification may be a more important mechanism at our site.

The positive hysteresis index values in the dry season suggest that the NO_3^- source is progressively removed (i.e., depleted) as it exchanges with the marsh platform (Figure 7). Previous work in salt marshes have highlighted that NO_3^- is imported from estuarine surface water into marsh porewater during tidal inundation (Wang *et al.*, 2022). Our results aligns with previous research showing that salt marsh systems can remove NO_3^-, thereby reducing the impacts of excess nutrients on nearshore waters (Hamersley and Howes, 2005; Bulseco *et al.*, 2019; Bowen *et al.*, 2020).

Variability in the hysteresis and flushing indices was more pronounced in wet periods than in dry periods (Figure 6). However, we did not find any relationship between *HI* and *FI* and the timing of precipitation events, terrestrial water level elevation, tidal elevation, surface water temperature, surface water pH, surface water salinity, or surface water turbidity (Figures S6, S7, S8). This finding suggests that the variability in *HI* and *FI* during the wet season is likely driven by other processes, such as other NO_3^- delivery or processing mechanisms that our analysis is unable to constrain. Future work will look at the combined effect of multiple, potentially interacting, environmental drivers in multivariate space.

Salt marshes are under pressure from chronic sea level rise, changing precipitation regimes, and increasing human activity around coastal environments (Krause *et al.*, 2020). These marked differences in the overall NO_3^- processing in the salt marsh as a function of seasonality may become more important with changing patterns in precipitation (Donat *et al.*, 2016). Climate change in California is projected to cause less frequent, but more intense precipitation events (Swain *et al.*, 2018), which has already been shown to affect salt marsh functionality (Russo *et al.*, 2013). Fewer, but more extreme precipitation events will likely result in relatively higher pulses of NO_3^- into the estuary during runoff events because NO_3^- can accumulate in the soil during extended rainless periods and get flushed during higher intensity storm events. Such predicted NO_3^- loads to Elkhorn Slough will test the potential of the salt marsh to remove pollutants and mitigate water quality issues in coastal systems. Additionally, changing precipitation regimes may also have an impact on seasonal groundwater contributions to the salt marsh, which may control the duration of wet and dry seasons and subsequent N processing.

5.2 Tides drove within marsh variation in porewater NO_3^-

Tidal inundation induced NO_3^- fluctuations at intra-tidal scales, but the amplitude of these variations differed between seasons. During the wet season, the tidal fluctuations of the NO_3^- time series were less evident (i.e., the distinct NO_3^- peaks at tidal frequencies were damped; Figure 3 A-B). When the terrestrial groundwater level was below the marsh surface in the dry season, we observed a stronger tidal signal in the NO_3^- record (Figure 3 C-D). We expected to find the opposite pattern (more significant fluctuations in pore water NO_3^- over wet season tidal cycles) because of higher NO_3^- concentrations in wet season surface water (Van Dop et al., 2019) and because NO_3^- is often limiting in marsh environments (Bledsoe et al., 2020). However, NO_3^- patterns in the dry season resulted in a more pronounced intra-tidal variation than the NO_3^--producing behavior in the wet season. Additionally, we observed within-marsh variation across tidal events, positions, and depths (Figures 3 and 5). Tidal events influenced porewater NO_3^- concentrations on hourly timescales across the study period, with distinct NO_3^- spikes (both positive and negative) at tidal frequencies across depths and marsh positions (e.g., Figures 3 and 6). These findings are consistent with previous measurements of high-frequency (1-minute resolution) redox potential and porewater level that suggested a relatively fast exchange of tidal water with porewater that influenced biogeochemical processes at intra-tidal timescales (Grande *et al.*, 2022a).

We observed a tidal "signature" consisting of a characteristic increase and subsequent decrease in porewater NO_3^- during inundation (Figures 3 and 6). One potential explanation of this signature is that NO_3^- in tidal surface water infiltrates into the marsh subsurface and is subsequently consumed by dissimilatory nitrate reduction processes such as denitrification or DNRA (Giblin *et al.*, 2013; Devol, 2015). Alternatively, Elkhorn Slough surface water has relatively elevated NH_4^+ concentration (Hicks *et al.*, 2019, Figure 5), which in combination with dissolved oxygen in tidal waters, can lead to nitrification in the marsh subsurface (i.e., the salt marsh can be a source of NO_3^-). The subsequent decrease in NO_3^- is likely caused by DNRA or denitrification. We observed small-scale within-marsh variation across positions and depths. Microbial processes such as DNRA or nitrification are tightly coupled to plant activity, oxygen concentrations, and substrate availability (Koop-Jakobsen and Wenzhöfer, 2015). Although our study does not disentangle the direct mechanisms causing variation in NO_3^- concentrations, our in situ high-frequency sensor measurements indicate that within-marsh processing exerts influence on net marsh NO_3^- export within the broader context of seasonal hydrologic drivers. Further, our findings highlight the importance of short-term and small spatial scale drivers of NO_3^- dynamics that might not be captured with point or synoptic measurements.

Precipitation events had short-term effects on observed salt marsh porewater NO_3^- concentrations (e.g., Figure S9). For example, in the October deployment, we found that the tidal effect appeared more muted in the NO_3^- time series during precipitation periods across all depths and marsh positions (shaded region in Figure S9). This finding suggests that precipitation water exchanged with salt marsh porewater, diluting the NO_3^- concentration. This result agrees with previous observations of multilevel decomposition of continuous redox potential measurements across this salt marsh transect during a precipitation event that showed precipitation water changed redox potential at depth (Grande et al., 2022). These interactions occur at relatively short timescales because we see a relatively instantaneous dilution pattern during the storm event in the NO_3^- time series that recovered quickly post event.

6. CONCLUSION

This study identified the role of multi-scale (intra-tidal and seasonal) hydrologic drivers on controlling porewater NO_3^- concentrations in a Mediterranean-climate salt marsh system, where water quality is a concern. Overall, the knowledge obtained from this analysis of NO_3^- hysteretic responses to tidal events provides valuable insight into solute-porewater level patterns and uses them to make inferences about the dominant biogeochemical processes driving them across seasons. The seasonal differences in NO_3^- dynamics occurring over sub-hourly timescales highlight the necessity of both long-term and high frequency continuous monitoring.

The hysteresis indices used in this study indicate that the salt marsh has different dominant transport and biogeochemical processing behavior in wet and dry seasonal periods (Figure 6). Overall, the salt marsh is most retentive during the dry season, and depletion and consumption patterns dominate during these periods. In contrast, the salt marsh is least retentive during the wet season when NO_3^- production dominates. This is particularly evident in the lower and upper marsh positions, where the salt marsh shifts between predominantly removing NO_3^- in dry periods and producing NO_3^- in wet periods.

The salt marsh is generally a net sink of estuarine derived NO_3^- during the dry season. However, here we showed that during the wet season, the salt marsh exports NO_3^- to the estuary, providing evidence that salt marshes may not always serve as nutrient sinks. Our observations suggest that salt marsh NO_3^- export may contribute to already-elevated estuarine surface water NO_3^- concentrations in wet seasons. The looser coupling of tidal cycles and NO_3^- concentrations in the wet season suggests that other NO_3^- sources may play a role during high groundwater levels. Specifically, our results hint at the potential role of groundwater or shallow subsurface storm flow in delivering NO_3^- to the salt marsh in the wet season.

Although biogeochemical cycling of NO_3^- and other nitrogen species in coastal wetlands have been studied extensively (Bowen *et al.*, 2020), NO_3^- processing at intra-tidal time scales across different depths is not often considered. The analysis presented here illustrates the potential benefit of continuous high-spatiotemporal resolution water quality observations data in combination with statistical methods to quantify tidal event hysteresis in salt marsh environments. c-Q analysis is a useful tool/framework that uses event-scale solute data to infer dominant behavior and process rates but does not measure these processes directly. However, the high-frequency observations can be used to target hot spots and hot moments of biogeochemical activity for additional mechanistic measurements and for informing predictions about biogeochemical responses to future response to environmental change.

Our future work will incorporate these high spatiotemporal field measurements of NO_3^- concentrations with additional monitoring data of salinity and isotopic fingerprints to understand mixing between terrestrial groundwater and inundation. An essential remaining step in the field is to implement these hydro-biogeochemical processes into reactive transport modeling to develop practical mechanistic understanding, including explaining the interactions between flow paths, residence times, and solute kinetics in coastal systems. We think that an integrative understanding of physical and biogeochemical processes will be crucial for managing salt marshes as NO_3^- enrichment and climate change continue to threaten our coasts.

ACKNOWLEDGEMENT

This study was conducted in Elkhorn Slough, unceded land of the Calandaru (people of “Bay Houses”). We recognize that this ancestral land was and continues to be of great importance to the local tribes and their descendants.

The authors sincerely thank Dan Sampson from the University of California Santa Cruz (UCSC) for his valuable help programming and installing the electronic devices used in this study. We also thank Dr. Brian Dreyer, director of the UCSC Marine Analytical Lab for help with sample analysis. We thank Maya Montalvo, Loren Tolley-Man, Michael Wilshire, and Andria Greene for field assistance. Grande was partially funded by a Cota-Robles Fellowship through the University of California Santa Cruz and by a NOAA Margaret A. Davidson fellowship (NA20NOS4200122). We acknowledge support from the NITRATES Project, funded by the U.S. Department of Energy Office of Biological and Environmental Research under Award Number DE-SC0021044. We acknowledge support from a California SeaGrant under California Natural Resources Agency Award Number C0303100.

DATA AVAILABILITY

The data used in this research is available through the Environmental System Science Data Infrastructure for a Virtual Ecosystem repository (ESS-DIVE) (Grande *et al.*, 2023)

REFERENCES

Aguilera R, Melack JM. 2018. Concentration-Discharge Responses to Storm Events in Coastal California Watersheds: C-Q STORM RESPONSES COASTAL CALIFORNIA. *Water Resources Research* **54** (1): 407–424 DOI: 10.1002/2017WR021578

Andrea B, Francesc G, Jérôme L, Eusebi V, Francesc S. 2006. Cross-site Comparison of Variability of DOC and Nitrate c–q Hysteresis during the Autumn–winter Period in Three Mediterranean Headwater Streams: A Synthetic Approach. *Biogeochemistry* **77** (3): 327–349 DOI: 10.1007/s10533-005-0711-7

Arora B, Burrus M, Newcomer M, Steefel CI, Carroll RWH, Dwivedi D, Dong W, Williams KH, Hubbard SS. 2020. Differential C-Q Analysis: A New Approach to Inferring Lateral Transport and Hydrologic Transients Within Multiple Reaches of a Mountainous Headwater Catchment. *Frontiers in Water* **2** Available at: https://www.frontiersin.org/article/10.3389/frwa.2020.00024 [Accessed 9 April 2022]

Beheshti K, Endris C, Goodwin P, Pavlak A, Wasson K. 2022. Burrowing crabs and physical factors hasten marsh recovery at panne edges. *PLOS ONE* **17** (1): e0249330 DOI: 10.1371/journal.pone.0249330

Bieroza MZ, Heathwaite AL. 2015. Seasonal variation in phosphorus concentration–discharge hysteresis inferred from high-frequency in situ monitoring. *Journal of Hydrology* **524**: 333–347 DOI: 10.1016/j.jhydrol.2015.02.036

Birgand F, Aveni-Deforge K, Smith B, Maxwell B, Horstman M, Gerling AB, Carey CC. 2016. First report of a novel multiplexer pumping system coupled to a water quality probe to collect high temporal frequency in situ water chemistry measurements at multiple sites: High-Resolution Water Chemistry in Time and Space. *Limnology and Oceanography: Methods* **14** (12): 767–783 DOI: 10.1002/lom3.10122

Bowen JL, Giblin AE, Murphy AE, Bulseco AN, Deegan LA, Johnson DS, Nelson JA, Mozdzer TJ, Sullivan HL. 2020. Not All Nitrogen Is Created Equal: Differential Effects of Nitrate and Ammonium Enrichment in Coastal Wetlands. *BioScience* **70** (12): 1108–1119 DOI: 10.1093/biosci/biaa140

Breslow N. 1970. A Generalized Kruskal-Wallis Test for Comparing K Samples Subject to Unequal Patterns of Censorship. *Biometrika* **57** (3): 579–594 DOI: 10.2307/2334776

Bulseco AN, Giblin AE, Tucker J, Murphy AE, Sanderman J, Hiller-Bittrolff K, Bowen JL. 2019. Nitrate addition stimulates microbial decomposition of organic matter in salt marsh sediments. *Global Change Biology*: gcb.14726 DOI: 10.1111/gcb.14726

Caetano M, Bernárdez P, Santos-Echeandia J, Prego R, Vale C. 2012. Tidally driven N, P, Fe and Mn exchanges in salt marsh sediments of Tagus estuary (SW Europe). *Environmental Monitoring and Assessment* **184** (11): 6541–6552 DOI: 10.1007/s10661-011-2439-2

Caffrey JM. 2002. Chapter 3: Climate. In *Changes in a California Estuary: An Ecosystem Profile of Elkhorn Slough*, Caffrey JM, , Brown M, , Tyler B, , Silberstain M (eds).Elkhorn Slough Fundation: Moss Landing, California; 25–28. Available at: http://library.elkhornslough.org/attachments/Caffrey_2002_Changes_In_A_California.pdf [Accessed 20 March 2022]

Caffrey JM, Broenkow W. 2002. Chapter 4: Hydrography. In *Changes in a California Estuary: An Ecosystem Profile of Elkhorn Slough*, Caffrey JM, , Brown M, , Tyler B, , Silberstain M (eds).Elkhorn Slough Fundation: Moss Landing, California; 29–42. Available at: http://library.elkhornslough.org/attachments/Caffrey_2002_Changes_In_A_California.pdf [Accessed 20 March 2022]

Caffrey JM, Harrington N, Ward B. 2002. Biogeochemical processes in a small California estuary. 1. Benthic fluxes and pore water constituents reflect high nutrient freshwater inputs. *Marine Ecology Progress Series* **233**: 39–53 DOI: 10.3354/meps233039

Chanat JG, Rice KC, Hornberger GM. 2002. Consistency of patterns in concentration-discharge plots: PATTERNS IN CONCENTRATION-DISCHARGE PLOTS. *Water Resources Research* **38** (8): 22-1-22–10 DOI: 10.1029/2001WR000971

Chapin TP, Caffrey JM, Jannasch HW, Coletti LJ, Haskins JC, Johnson KS. 2004. Nitrate sources and sinks in Elkhorn Slough, California: Results from long-term continuous in situ nitrate analyzers. *Estuaries* **27** (5): 882–894 DOI: 10.1007/BF02912049

Devol AH. 2015. Denitrification, Anammox, and N2 Production in Marine Sediments. *Annual Review of Marine Science* **7** (1): 403–423 DOI: 10.1146/annurev-marine-010213-135040

Donat MG, Lowry AL, Alexander LV, O'Gorman PA, Maher N. 2016. More extreme precipitation in the world's dry and wet regions. *Nature Climate Change* **6** (5): 508–513 DOI: 10.1038/nclimate2941

Etheridge JR, Birgand F, Osborne JA, Osburn CL, Burchell MR, Irving J. 2014. Using in situ ultraviolet-visual spectroscopy to measure nitrogen, carbon, phosphorus, and suspended solids concentrations at a high frequency in a brackish tidal marsh: In situ spectroscopy to monitor N, C, P, TSS. *Limnology and Oceanography: Methods* **12** (1): 10–22 DOI: 10.4319/lom.2014.12.10

Fox J, Weisberg S. 2019. *An R Companion to Applied Regression*. Sage: Thousand Oaks, CA\. Available at: https://socialsciences.mcmaster.ca/jfox/Books/Companion/

Gastwirth JL, Gel YR, Miao W. 2009. The Impact of Levene's Test of Equality of Variances on Statistical Theory and Practice. *Statistical Science* **24** (3): 343–360 DOI: 10.1214/09-STS301

Giblin A, Tobias C, Song B, Weston N, Banta G, Rivera-Monroy V. 2013. The Importance of Dissimilatory Nitrate Reduction to Ammonium (DNRA) in the Nitrogen Cycle of Coastal Ecosystems. *Oceanography* **26** (3): 124–131 DOI: 10.5670/oceanog.2013.54

Gleeson J, Santos IR, Maher DT, Golsby-Smith L. 2013. Groundwater–surface water exchange in a mangrove tidal creek: Evidence from natural geochemical tracers and implications for nutrient budgets. *Marine Chemistry* **156**: 27–37 DOI: 10.1016/j.marchem.2013.02.001

Grande E, Arora B, Visser A, Montalvo M, Braswell A, Seybold E, Tatariw C, Beheshti K, Zimmer M. 2022a. Tidal frequencies and quasiperiodic subsurface water level variations dominate redox dynamics in a salt marsh system. *Hydrological Processes* **36** (5): 1–16 DOI: 10.1002/hyp.14587

Grande E, Arora B, Zimmer M. 2022b. Subsurface redox potential and water level at the Elkhorn Slough NERR. DOI: 10.15485/1846282. Environmental System Science Data Infrastructure for a Virtual Ecosystem (ESS-DIVE) (United States). DOI: 10.15485/1846282

Grande E, Visser A, Beitz P, Moran J. 2019. Examination of Nutrient Sources and Transport in a Catchment with an Audubon Certified Golf Course. *Water* **11** (9): 1923 DOI: 10.3390/w11091923

Grande E, Zimmer M, Seybold E, Tatariw C. 2023. Modeled sub-hourly nitrate concentrations in subsurface water across a salt marsh system in Elkhorn Slough, California Available at: https://data.ess-dive.lbl.gov/view/doi:10.15485/1987518 [Accessed 3 July 2023]

Hamersley MR, Howes BL. 2005. Coupled nitrification–denitrification measured in situ in a Spartina alterniflora marsh with a 15NH4+ tracer. *Marine Ecology Progress Series* **299**: 123–135 DOI: 10.3354/meps299123

Hicks K, Jeppesen R, Haskins J, Wasson K. 2019. Long-term trends and spatial patterns of water quality in estuarine wetlands of central California. Elkhorn Slough Technical Report Series. Scientific Report 2019:1. Elkohrn Slough NERR, Moss Landing, California. Available at: http://library.elkhornslough.org/research/bibliography/Hicks_2019_Long-term_trends_and_spatial.pdf [Accessed 11 April 2022]

Hughes BB, Haskins JC, Wasson K, Watson E. 2011. Identifying factors that influence expression of eutrophication in a central California estuary. *Marine Ecology Progress Series* **439**: 31–43 DOI: 10.3354/meps09295

Jeppesen R, Rodriguez M, Rinde J, Haskins J, Hughes B, Mehner L, Wasson K. 2018. Effects of Hypoxia on Fish Survival and Oyster Growth in a Highly Eutrophic Estuary. *Estuaries and Coasts* **41** (1): 89–98 DOI: 10.1007/s12237-016-0169-y

Kincaid DW, Seybold EC, Adair EC, Bowden WB, Perdrial JN, Vaughan MCH, Schroth AW. 2020. Land Use and Season Influence Event-Scale Nitrate and Soluble Reactive Phosphorus Exports and Export Stoichiometry from Headwater Catchments. *Water*

Resources Research **56** (10): e2020WR027361 DOI: https://doi.org/10.1029/2020WR027361

Koop-Jakobsen K, Wenzhöfer F. 2015. The Dynamics of Plant-Mediated Sediment Oxygenation in Spartina anglica Rhizospheres—a Planar Optode Study. *Estuaries and Coasts* **38** (3): 951–963 DOI: 10.1007/s12237-014-9861-y

Krause JR, Watson EB, Wigand C, Maher N. 2020. Are Tidal Salt Marshes Exposed to Nutrient Pollution more Vulnerable to Sea Level Rise? *Wetlands* **40** (5): 1539–1548 DOI: 10.1007/s13157-019-01254-8

Kumar P, Dasgupta R, Johnson BA, Saraswat C, Basu M, Kefi M, Mishra BK. 2019. Effect of Land Use Changes on Water Quality in an Ephemeral Coastal Plain: Khambhat City, Gujarat, India. *Water* **11** (4): 724 DOI: 10.3390/w11040724

Liland KH, Mevik B, Wehrens R, Hiemstra P. 2021. pls: Partial Least Squares and Principal Component Regression Available at: https://github.com/khliland/pls

Liu W, Birgand F, Tian S, Chen C. 2021. Event-scale hysteresis metrics to reveal processes and mechanisms controlling constituent export from watersheds: A review☆. *Water Research* **200**: 117254 DOI: 10.1016/j.watres.2021.117254

Liu W, Youssef MA, Birgand FP, Chescheir GM, Tian S, Maxwell BM. 2020. Processes and mechanisms controlling nitrate dynamics in an artificially drained field: Insights from high-frequency water quality measurements. *Agricultural Water Management* **232**: 106032 DOI: 10.1016/j.agwat.2020.106032

Lloyd CEM, Freer JE, Johnes PJ, Collins AL. 2016. Using hysteresis analysis of high-resolution water quality monitoring data, including uncertainty, to infer controls on nutrient and sediment transfer in catchments. *Science of The Total Environment* **543**: 388–404 DOI: 10.1016/j.scitotenv.2015.11.028

Malzone CM. 1999. Tidal scour and its relation to erosion and sediment transport in Elkhorn Slough.Master Thesis, San Jose State University, San Jose, California, United States.

O'Dell JW. 1996. DETERMINATION OF NITRATE-NITRITE NITROGEN BY AUTOMATED COLORIMETRY. In *Methods for the Determination of Metals in Environmental Samples*Elsevier; 464–478. DOI: 10.1016/B978-0-8155-1398-8.50026-4

Oeurng C, Sauvage S, Sánchez-Pérez J-M. 2010. Temporal variability of nitrate transport through hydrological response during flood events within a large agricultural catchment in south-west France. *Science of The Total Environment* **409** (1): 140–149 DOI: 10.1016/j.scitotenv.2010.09.006

Peterson RN, Moore WS, Chappel SL, Viso RF, Libes SM, Peterson LE. 2016. A new perspective on coastal hypoxia: The role of saline groundwater. *Marine Chemistry* **179**: 1–11 DOI: 10.1016/j.marchem.2015.12.005

R Core Team. 2021. R: A language and environment for statistical computing. R Foundation for Statistical Computing Available at: https://www.R-project.org/

Reading MJ, Santos IR, Maher DT, Jeffrey LC, Tait DR. 2017. Shifting nitrous oxide source/sink behaviour in a subtropical estuary revealed by automated time series observations. *Estuarine, Coastal and Shelf Science* **194**: 66–76 DOI: 10.1016/j.ecss.2017.05.017

Robinson CE, Xin P, Santos IR, Charette MA, Li L, Barry DA. 2018. Groundwater dynamics in subterranean estuaries of coastal unconfined aquifers: Controls on submarine groundwater discharge and chemical inputs to the ocean. *Advances in Water Resources* **115**: 315–331 DOI: 10.1016/j.advwatres.2017.10.041

Rosner B, Grove D. 1999. Use of the Mann–Whitney U-test for clustered data. *Statistics in Medicine* **18** (11): 1387–1400 DOI: 10.1002/(SICI)1097-0258(19990615)18:11<1387::AID-SIM126>3.0.CO;2-V

Russo TA, Fisher AT, Winslow DM. 2013. Regional and local increases in storm intensity in the San Francisco Bay Area, USA, between 1890 and 2010: STORM INTENSITY IN THE SFBA. *Journal of Geophysical Research: Atmospheres* **118** (8): 3392–3401 DOI: 10.1002/jgrd.50225

Santos IR, Eyre BD, Huettel M. 2012. The driving forces of porewater and groundwater flow in permeable coastal sediments: A review. *Estuarine, Coastal and Shelf Science* **98**: 1–15 DOI: 10.1016/j.ecss.2011.10.024

Schultz BB. 1985. Levene's Test for Relative Variation. *Systematic Biology* **34** (4): 449–456 DOI: 10.1093/sysbio/34.4.449

Shapiro SS, Wilk MB. 1965. An Analysis of Variance Test for Normality (Complete Samples). *Biometrika* **52** (3/4): 591–611 DOI: 10.2307/2333709

Sinha E, Michalak AM, Balaji V. 2017. Eutrophication will increase during the 21st century as a result of precipitation changes. *Science* **357** (6349): 405–408 DOI: 10.1126/science.aan2409

Slomp CP, Van Cappellen P. 2004. Nutrient inputs to the coastal ocean through submarine groundwater discharge: controls and potential impact. *Journal of Hydrology* **295** (1): 64–86 DOI: 10.1016/j.jhydrol.2004.02.018

Swain DL, Langenbrunner B, Neelin JD, Hall A. 2018. Increasing precipitation volatility in twenty-first-century California. *Nature Climate Change* **8** (5): 427–433 DOI: 10.1038/s41558-018-0140-y

Van Dop M, Hall A, Calhoun K, Kislik C. 2019. Linking land cover and water quality in Elkhorn Slough. Elkhorn Slough Technical Report Series. Elkhorn Slough, CA. Available at: http://library.elkhornslough.org/attachments/VanDop_2019_Linking_Land_Cover_And.pdf [Accessed 11 April 2022]

Van Dyke E, Wasson K. 2005. Historical ecology of a central California estuary: 150 years of habitat change. *Estuaries* **28** (2): 173–189 DOI: 10.1007/BF02732853

Vaughan MCH, Bowden WB, Shanley JB, Vermilyea A, Sleeper R, Gold AJ, Pradhanang SM, Inamdar SP, Levia DF, Andres AS, et al. 2017. High-frequency dissolved organic carbon and nitrate measurements reveal differences in storm hysteresis and loading in relation to land cover and seasonality. *Water Resources Research* **53** (7): 5345–5363 DOI: 10.1002/2017WR020491

Wang F, Xiao K, Santos IR, Lu Z, Tamborski J, Wang Y, Yan R, Chen N. 2022. Porewater exchange drives nutrient cycling and export in a mangrove-salt marsh ecotone. *Journal of Hydrology* **606**: 127401 DOI: 10.1016/j.jhydrol.2021.127401

Woolfolk A, Labadie Q. 2012. The significance of pickleweed-dominated tidal salt marsh in Elkhorn Slough, California: A literature review. Technical Report Series. Elkhorn Slough.

Zuecco G, Penna D, Borga M, van Meerveld HJ. 2016. A versatile index to characterize hysteresis between hydrological variables at the runoff event timescale: A Hysteresis

Index for Variables at the Runoff Event Timescale. *Hydrological Processes* **30** (9): 1449–1466 DOI: 10.1002/hyp.10681

List of Figures:

Figure 1. (A) Map of Elkhorn Slough with the extent of wetlands outlined in light blue. The black symbol marks the location of the study transect. The red symbol marks the location of the Kirby Park sampling station, where the ESNERR collects monthly estuarine surface water samples that are analyzed for NO_3^- and NH_4^+ concentration. (B) Map view of the experimental transect showing the location of the upland monitoring piezometer in relation to the salt marsh transect. (C) Conceptual figure showing a cross section of the experimental transect and showing the spatial distribution of the sampling cups (pink bars) and observation wells (blue bars) with a contour plot overlay of interpolated sediment bulk density across the salt marsh. The darker the colors in the contour plot, the greater the bulk density. The elevation (m amsl; not shown in the figure) of the salt marsh positions are: 1.79 m, 1.65 m, and 1.55 m for the upper, middle, and lower marsh, respectively.

Figure 2. Water level time series illustrating the seasonal variations of the terrestrial groundwater level (dark blue) as measured from the upland study location. The Mediterranean climate of the study area, with marked seasonality in precipitation (gray hanging bars), results in a drop of 1.34 m in the terrestrial groundwater level between the rainy and dry seasons. The figure also illustrates the porewater level time series in the upper (yellow), middle (light blue), and lower (pink) marsh positions. The horizontal dashed lines represent the salt marsh elevation at each marsh position (by color). The shaded regions mark the instrumentation deployment periods.

Figure 3. Plot of sub-hourly porewater NO_3^- concentrations from ~4 days during two deployment periods (March 9-12 and September 14-18 2021) from the 50 cm depth at the lower (A and C) and upper (B and D) marsh positions. The shaded regions represent the time intervals that were delineated for individual tidal events. The horizontal dashed lines mark the elevation of the salt marsh platform. The porewater level measured in observation wells at each marsh

position is shown in pink, and captures the local tidal cycle response. The terrestrial groundwater level measured at an upland position (navy blue line) is shown to highlight the "wetness" of the system as well as the elevation of the terrestrial groundwater with respect to the salt marsh elevation (e.g., high during the wet season and low during the dry season). The light blue envelope on the NO_3^- time series represents the uncertainty of the measurement at 95% confidence level of a linear regression between lab-measurements and the optical probe predictions.

Figure 4. Plots of (A) normalized NO_3^- concentration and normalized water level , (B) hysteresis index (HI), and (C) flushing index (FI;) for a tidal event at the lower marsh position (10 cm depth) on September 19th, 2021. We calculated hysteresis index HI_j (vertical dashed black lines in A) by subtracting the normalized NO_3^- on the falling limb from that of the rising limb for each 1 % of the normalized water level (as illustrated by the dotted lines on A). The event HI is the mean HI_j. The FI is the slope of the line that intersects the normalized NO_3^- concentration at the beginning and the point of peak water level for each tidal event (C). In this example HI = -0.091 and FI = -0.19.

Figure 5. (A) Violin plot of porewater NO_3^- concentrations across the three marsh positions considering all depths. (B) Marsh porewater NO_3^- concentration at 10, 30, and 50 cm depths for all marsh positions. (C) Violin plot of NO_3^- and NH_4^+ concentrations from surface water in the ESNERR for the 2021 calendar year. (D), (E), and (F) NO_3^- concentrations across depths for each marsh position. (G) NO_3^- concentration across the three marsh positions separated by dry (red) and wet seasons (blue). (H) NO_3^- concentration across the three depths separated by dry (red) and wet seasons (blue). One sample in (C) exceeded the 1 mg/L limit of the y axis with a concentration of 2.9 mg/L and was collected in February 2021. Asterisks on top of the plot designate significant differences (p-value < 0.05). All plot ordinates are on the same scale.

Figure 6. Split violin plots of the (A) tidal event flushing index and (B) hysteresis index for the lower, middle, and upper marsh positions, separated by dry (red) and wet (blue) seasons. The split violin plots show the distribution of hysteresis index values across all tidal events. The black

line in each violin plot marks the median of the distribution. (C) The hysteresis index versus flushing index for the 158 tidal events for the lower (circles; 58 events), middle (triangles; 43 events), and upper marsh (squares; 57 events) positions. Separating the hysteresis indices by dry (red) and wet (blue) seasons results in significant differences between these metrics.

Figure 7. Conceptual model of multi-scale hydrologic drivers (tidal and seasonal) in the salt marsh highlighting the shifts in the biochemical behavior of the salt marsh between wet (A-B) and dry (C-D) seasons. Counterclockwise loops and producing patterns in the wet season indicate that the salt marsh is a NO_3^- *source. Clockwise loops and depleting patterns in the dry season show that in this season, the salt marsh is a* NO_3^- *sink. Notice that surface water nutrient concentrations (*NO_3^-*,* NH_4^+*) are higher during the wet season.*

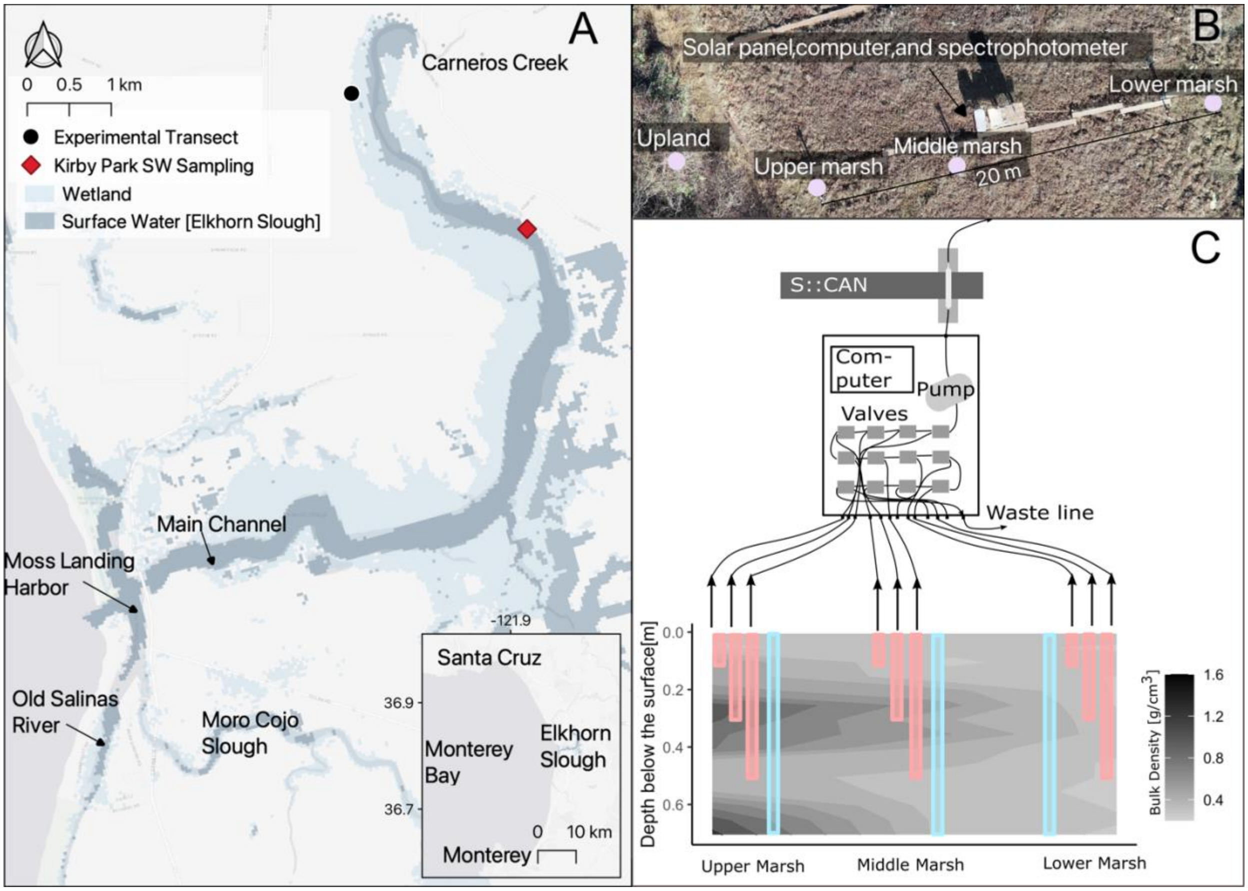
A
0 0.5 1 km
Experimental Transect
Kirby Park SW Sampling
Wetland
Surface Water [Elkhorn Slough]
Carneros Creek
Main Channel
Moss Landing Harbor
Old Salinas River
Moro Cojo Slough
-121.9
Santa Cruz
36.9
Monterey Bay
Elkhorn Slough
36.7
0 10 km
Monterey
B
Solar panel,computer,and spectrophotometer
Lower marsh
Upland
Middle marsh
Upper marsh
20 m
C
S::CAN
Com-puter
Pump
Valves
Waste line
Depth below the surface[m]
0.0
0.2
0.4
0.6
Bulk Density [g/cm3]
1.6
1.2
0.8
0.4
Upper Marsh
Middle Marsh
Lower Marsh

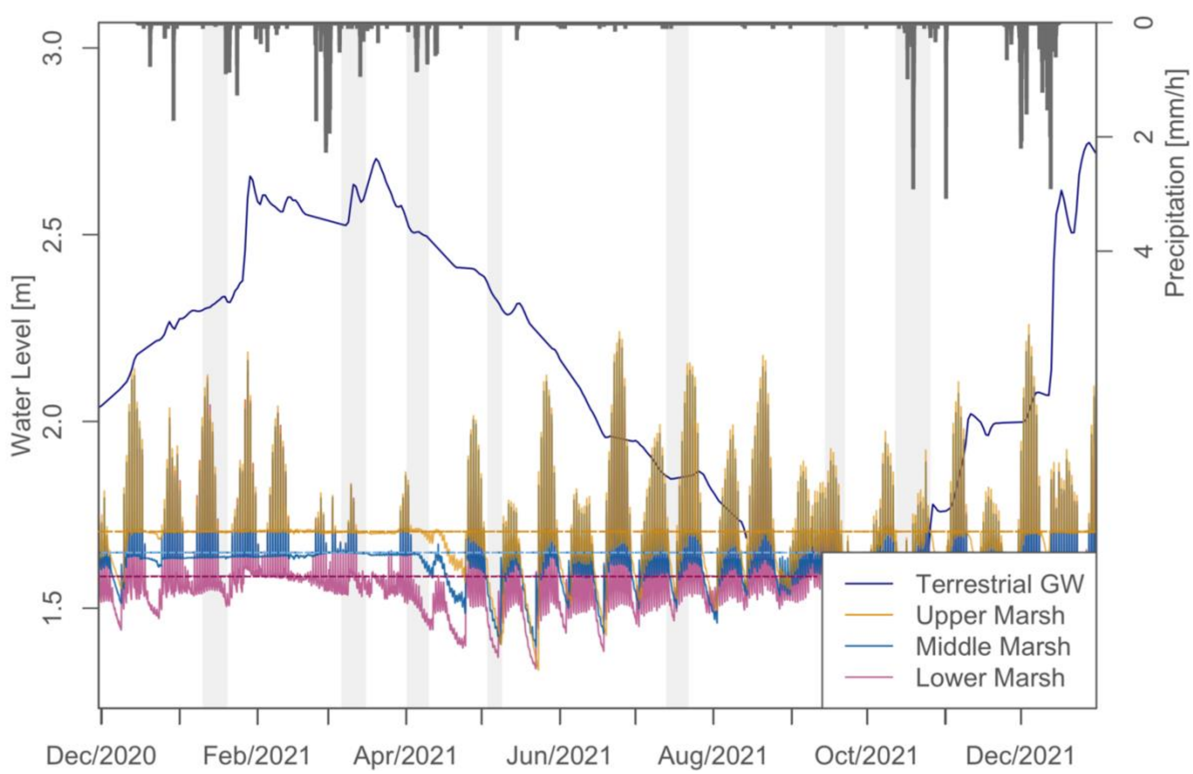
Water Level [m]
3.0
2.5
2.0
1.5
Precipitation [mm/h]
0
2
4
Terrestrial GW
Upper Marsh
Middle Marsh
Lower Marsh
Dec/2020
Feb/2021
Apr/2021
Jun/2021
Aug/2021
Oct/2021
Dec/2021

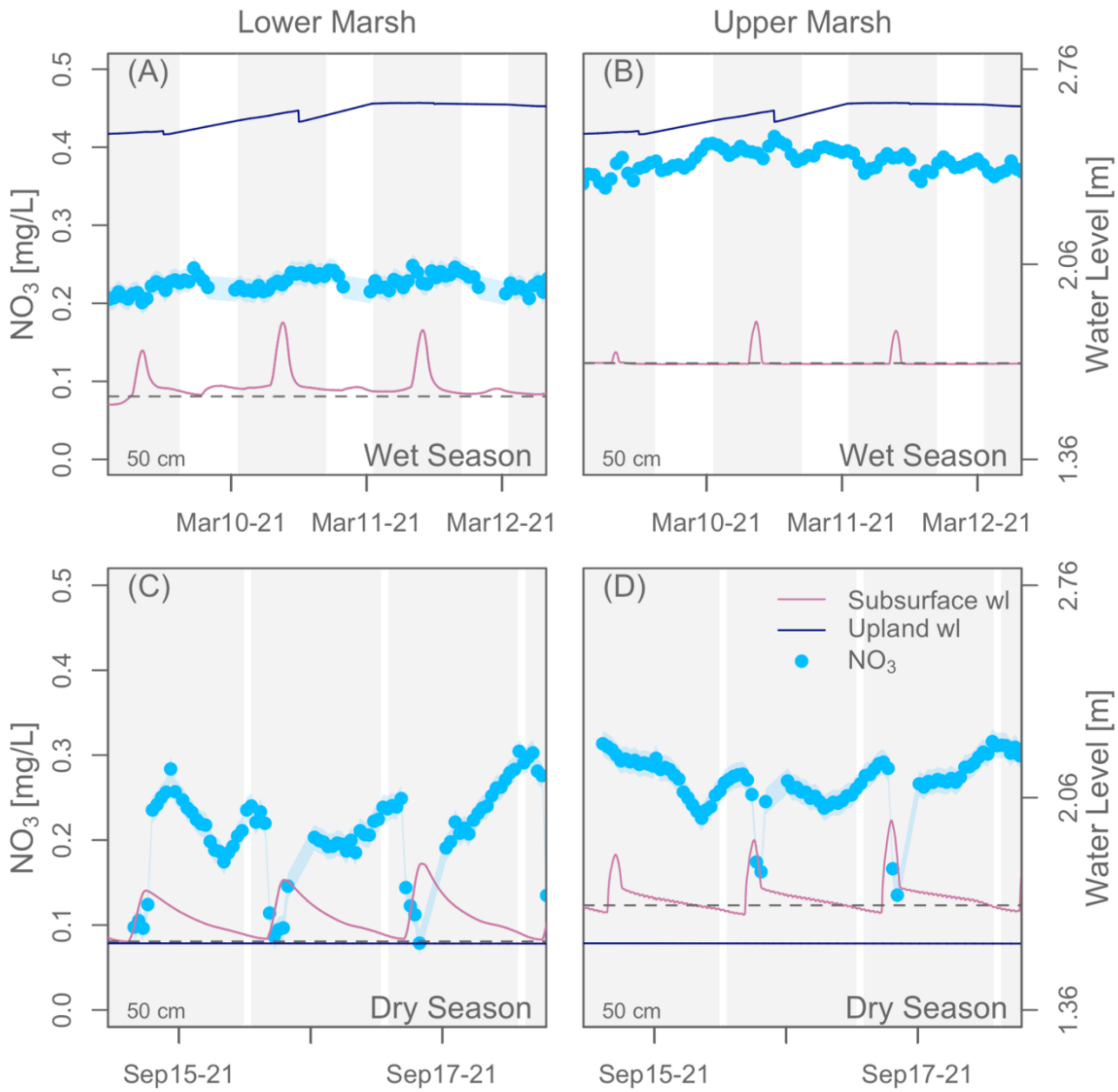
Lower Marsh
Upper Marsh
(A)
(B)
(C)
(D)
NO3 [mg/L]
Water Level [m]
0.0
0.1
0.2
0.3
0.4
0.5
1.36
2.06
2.76
50 cm
Wet Season
Dry Season
Mar10-21
Mar11-21
Mar12-21
Sep15-21
Sep17-21
Subsurface wl
Upland wl
NO3

871

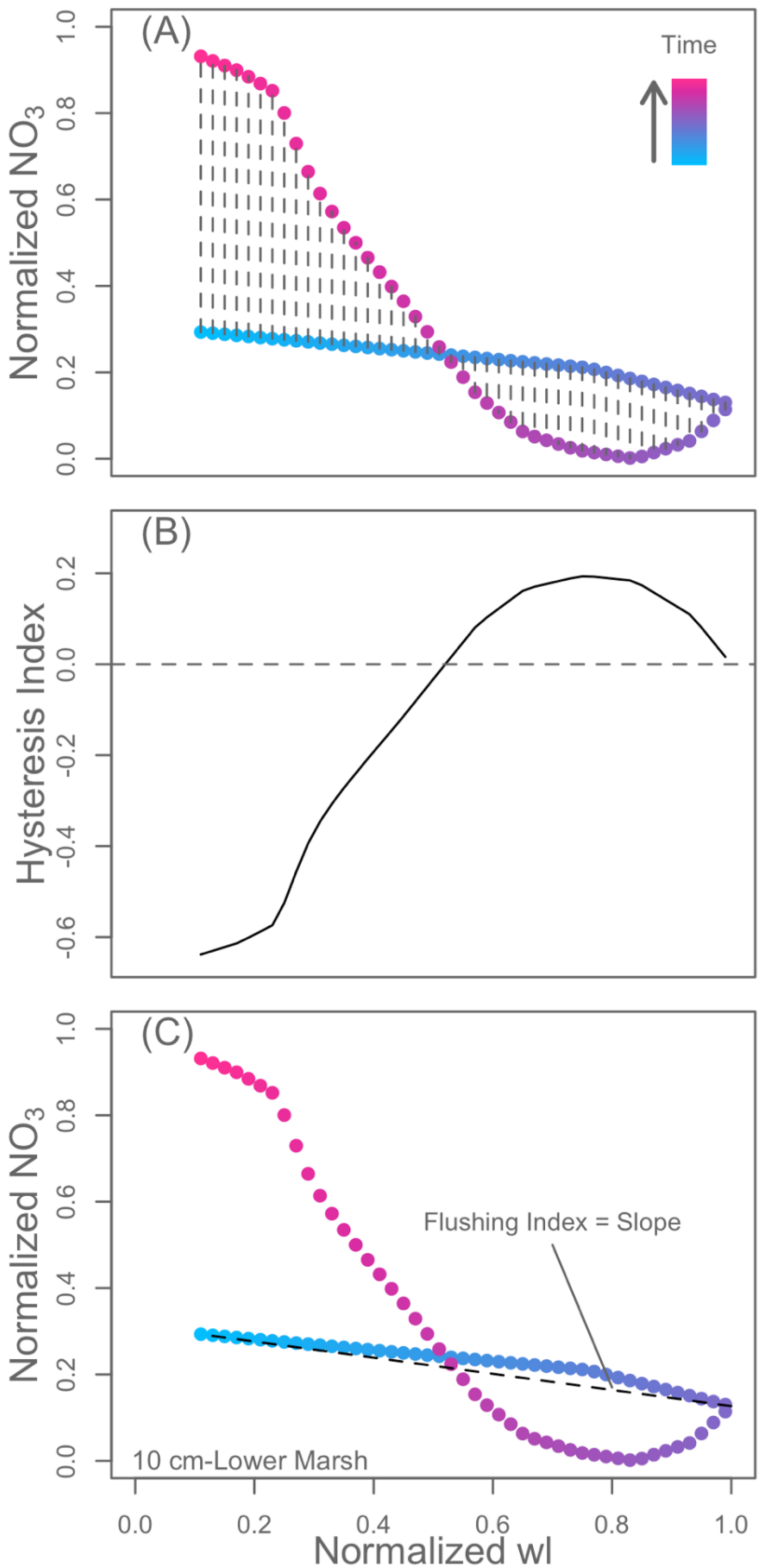
(A)
Time
Normalized NO_3
1.0
0.8
0.6
0.4
0.2
0.0
(B)
Hysteresis Index
0.2
0.0
-0.2
-0.4
-0.6
(C)
Flushing Index = Slope
10 cm-Lower Marsh
Normalized NO_3
0.0
0.2
0.4
0.6
0.8
1.0
Normalized wl

872

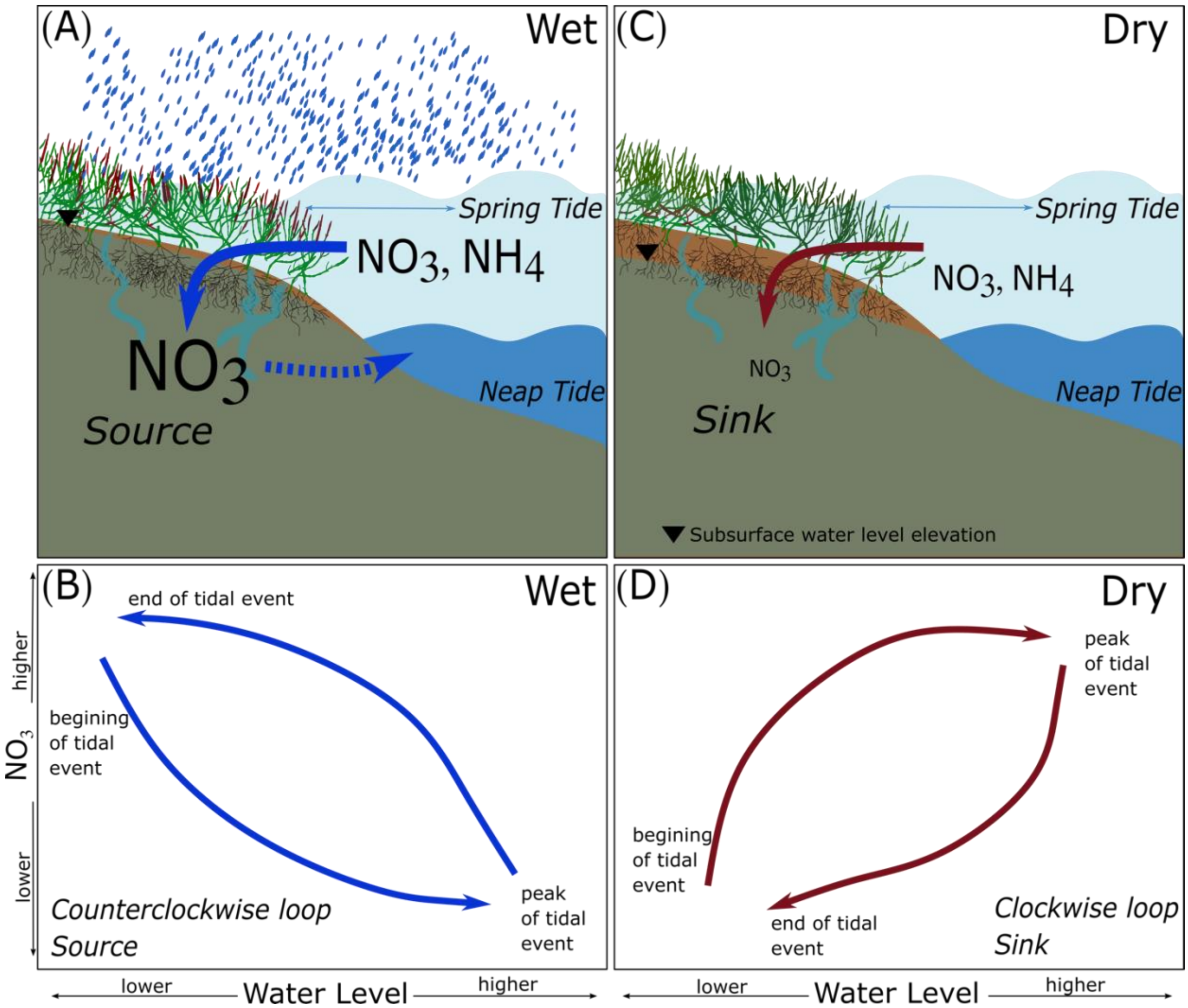

(A)
Wet
Spring Tide
NO3, NH4
NO3
Neap Tide
Source
(C)
Dry
Spring Tide
NO3, NH4
NO3
Neap Tide
Sink
Subsurface water level elevation
(B)
Wet
end of tidal event
begining of tidal event
peak of tidal event
Counterclockwise loop
Source
higher
NO3
lower
(D)
Dry
peak of tidal event
begining of tidal event
end of tidal event
Clockwise loop
Sink
lower
Water Level
higher
lower
Water Level
higher

874

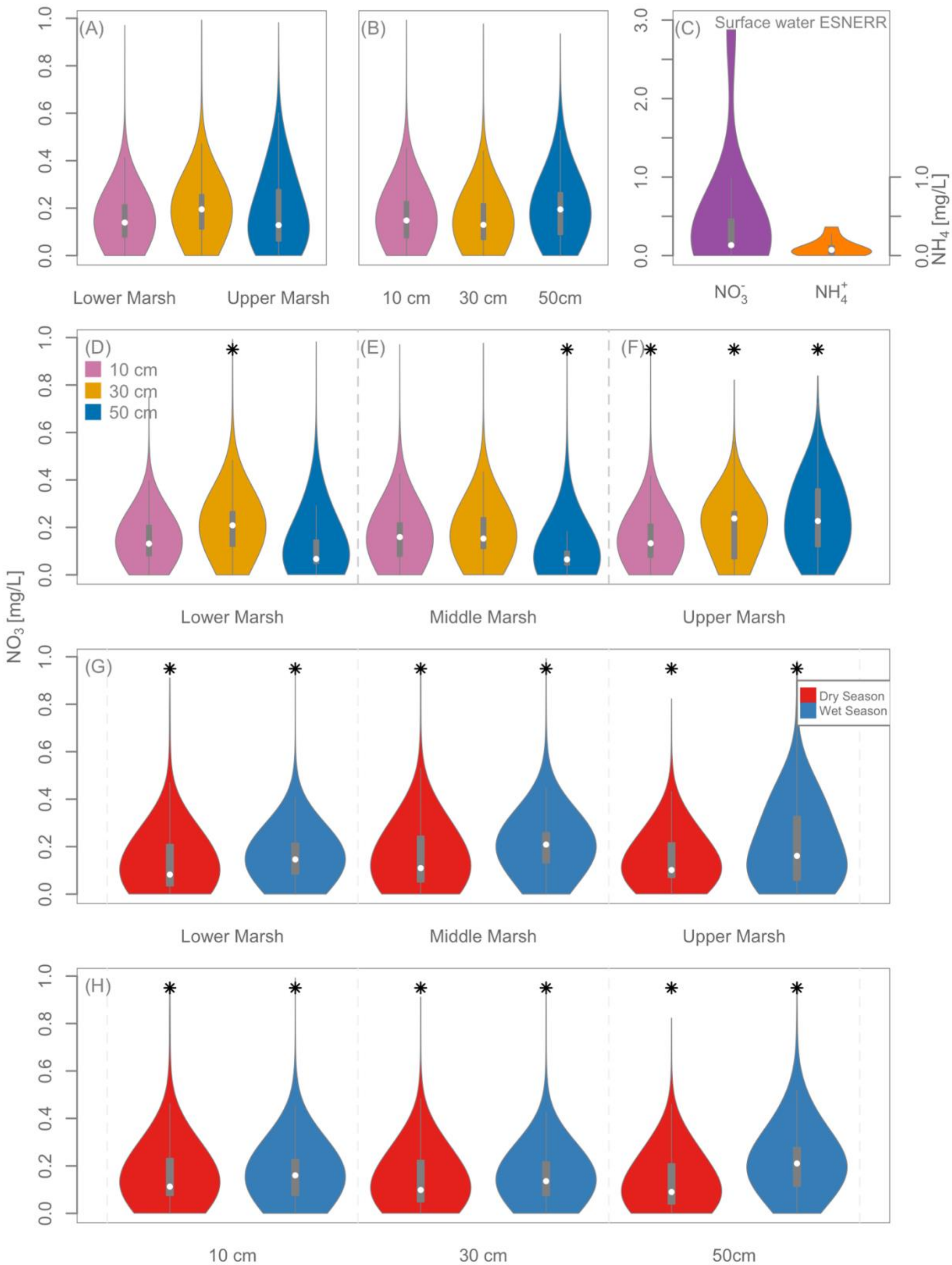

(A)
Lower Marsh
Upper Marsh
(B)
10 cm
30 cm
50cm
(C)
Surface water ESNERR
NO_3^-
NH_4^+
NH_4 [mg/L]
(D)
10 cm
30 cm
50 cm
(E)
(F)
Lower Marsh
Middle Marsh
Upper Marsh
NO_3 [mg/L]
(G)
Dry Season
Wet Season
Lower Marsh
Middle Marsh
Upper Marsh
(H)
10 cm
30 cm
50cm

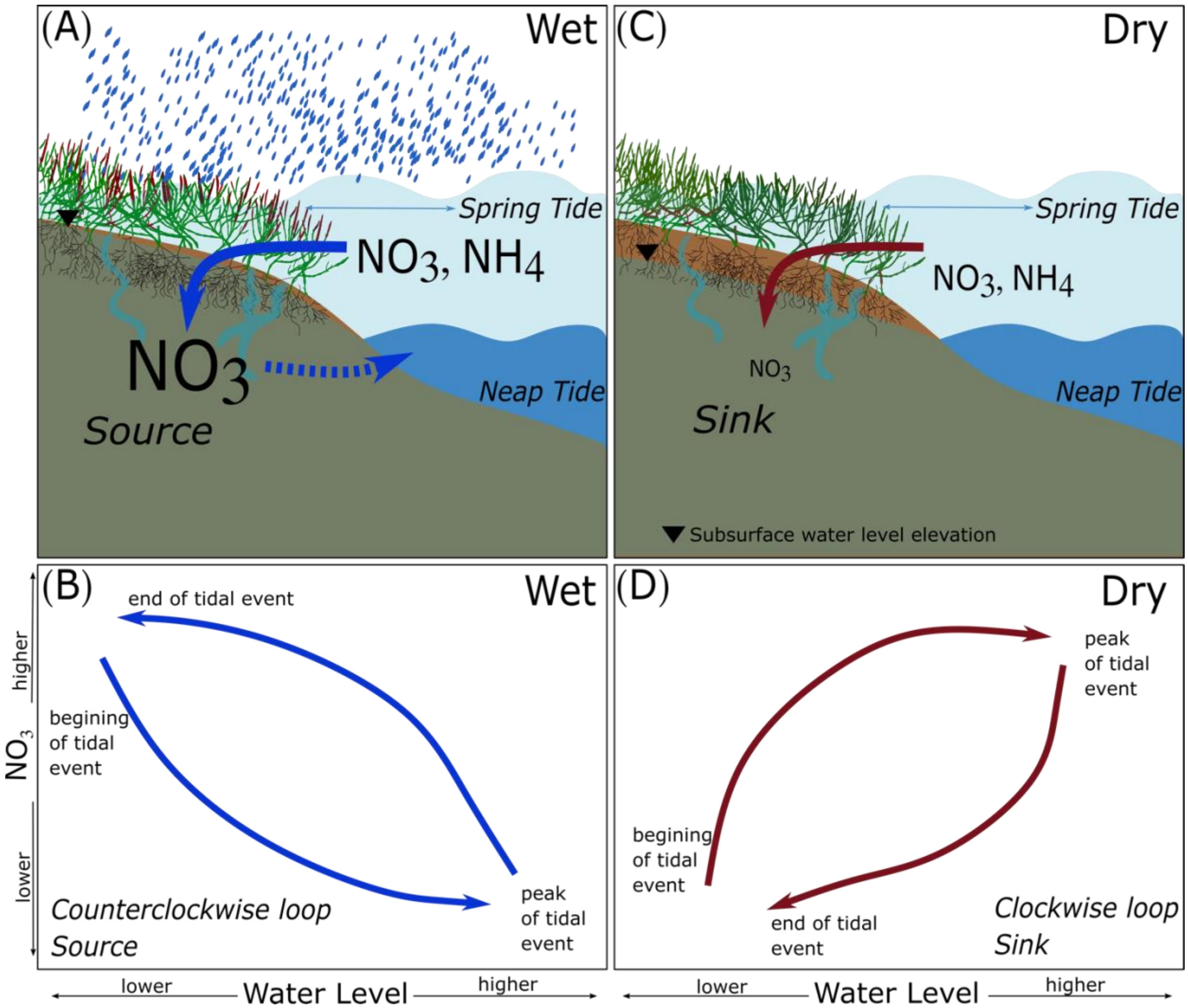

(A)
Wet
Spring Tide
NO_3, NH_4
NO_3
Neap Tide
Source
(C)
Dry
Spring Tide
NO_3, NH_4
NO_3
Neap Tide
Sink
Subsurface water level elevation
(B)
Wet
end of tidal event
begining of tidal event
peak of tidal event
Counterclockwise loop
Source
NO_3
higher
lower
(D)
Dry
peak of tidal event
begining of tidal event
end of tidal event
Clockwise loop
Sink
lower
Water Level
higher
lower
Water Level
higher

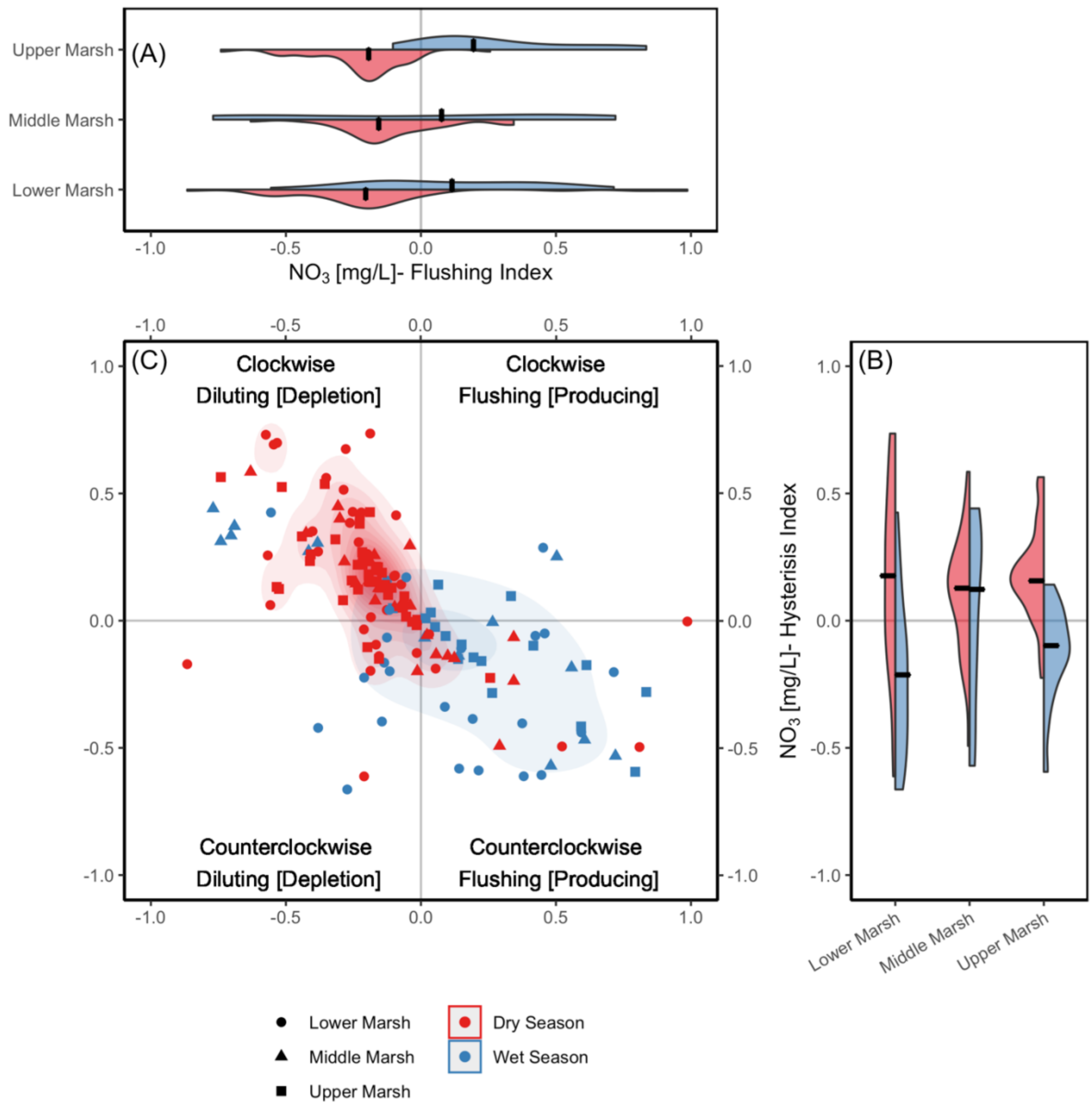

Marsh Position	Mean NO_3^- [mg/L]	Median NO_3^- [mg/L]	SD NO_3^- [mg/L]	IQR NO_3^- [mg/L]
Lower	0.15	0.14	0.10	0.14
Middle	0.19	0.19	0.12	0.151
Upper	0.18	0.14	0.15	0.22

Depth [cm]				
10	0.167	0.15	0.12	0.15
30	0.15	0.13	0.11	0.15
50	0.20	0.19	0.13	0.18

Table 1. Summary statistics for the different marsh positions and across all depths of the experimental transect. SD is the standard deviation and IQR is the interquartile range (i.e., the range between the 25th and 75th quartiles).

Marsh Position	Median dry season NO_3^- [mg/L]	Median wet season NO_3^- [mg/L]	Kruskal-Wallis test: H
Lower	0.08	0.19	507.6
Middle	0.11	0.24	499.4
Upper	0.10	0.17	104.4
Depth [cm]			
10	0.11	0.20	144.5
30	0.10	0.18	183.7
50	0.09	0.24	1198.6

Table 2. Summary statistics of seasonal salt marsh porewater NO_3^- concentrations. Wet season NO_3^- concentrations are significantly higher in all the marsh positions and depths of this study. All tests in the table have 1 degree of freedom and p-value < 0.0001.

Marsh Position	Depth [cm]	Median dry season NO_3 [mg/L]	Median wet season NO_3 [mg/L]	Kruskal-Wallis test: H

Lower	10	0.13	0.19	83.1
Lower	30	0.09	0.19	110.4
Lower	50	0.04	0.20	339.4
Middle	10	0.12	0.24	184.0
Middle	30	0.12	0.22	155.4
Middle	50	0.07	0.25	144.4
Upper	10	0.11	0.06	158.5
Upper	30	0.10	0.05	470.1
Upper	50	0.10	0.34	144.4

Table 3. Summary statistics of seasonal effects on NO_3^- concentrations by depth in each marsh position. All tests in the table have 1 degree of freedom and p-value < 0.0001.

Marsh Position	Depth [cm]	median dry season *HI*	median wet season *HI*	Kruskal-Wallis test: H	p-value
Lower	10	0.14	-0.03	6.4	0.01
Lower	30	0.36	0.16	0.5	0.5
Lower	50	0.06	-0.2	4.4	0.04
Middle	10	0.16	0.37	3.8	0.05
Middle	30	0.06	-0.16	2.7	0.1
Middle	50	0.10	0.27	1.4	0.2
Upper	10	0.21	-0.28	10.8	0.001

Upper	30	0.18	0.01	7.4	0.006
Upper	50	0.13	-0.06	4.5	0.03
		median dry season *FI*	median wet season *FI*	Kruskal-Wallis test: H	p-value
Lower	10	-0.17	0.04	6.4	0.07
Lower	30	-0.22	-0.13	0.1	0.7
Lower	50	-0.21	0.46	4.9	0.03
Middle	10	-0.19	-0.74	6.2	0.01
Middle	30	-0.04	0.37	3.3	0.07
Middle	50	-0.17	-0.42	0.4	0.5
Upper	10	-0.22	-0.26	13.0	0.001
Upper	30	-0.19	0.06	9.0	0.003
Upper	50	-0.18	0.33	9.3	0.002

Table 4. Summary statistics of seasonal effects on hysteresis index (HI) and flushing index (FI) by depth in each marsh position. Significant differences in wet/dry seasons are marked by bolded p-values in the table. All tests in the table have 1 degree of freedom.